Seismic moment tensor inversion using a 3-D structural model: applications for the Australian region

Myall Hingee,[1] Hrvoje Tkalčić,[2] Andreas Fichtner[2] and Malcolm Sambridge[1]

[1]*Research School of Earth Sciences, The Australian National University, Acton,* ACT 0200, *Australia. E-mail: Hrvoje.Tkalcic@anu.edu.au*
[2]*Department of Earth Sciences, Utrecht University,* 3508 *TA Utrecht, Netherlands*

SUMMARY

There is significant seismic activity in the region around Australia, largely due to the plate boundaries to the north and to the east of the mainland. This activity results in serious seismic and tsunami hazard in the coastal areas of Australia. Hence seismicity is and will be monitored in real time by Geoscience Australia (GA), which uses a network of permanent broadband seismometers. Seismic moment tensor (MT) solutions are currently determined using 1-D, radially symmetric models of Earth and this requires augmentation by recording stations located outside of Australia. A 3-D model of the Australian continent developed recently using full waveform tomography now offers the opportunity to significantly improve the determination of MT solutions of earthquakes from tectonically active regions. A complete-waveform, time-domain MT inversion method has been developed using a point-source approximation. A series of synthetic tests using first a 1-D and then a 3-D structural model has been performed. The feasibility of deploying 3-D versus 1-D Earth structure for the inversion of seismic data has been studied and the advantages of using the 3-D structural model were illustrated with examples. The 3-D model is superior to the 1-D model, as a number of sensitivity tests show. The ultimate goal of this work is an automated MT inversion system in Australia relying on GA and other international stations, although more work remains to be done before the full implementation of such a scheme in real time.

Key words: Earthquake source observations; Wave propagation; Early warning.

GJI Seismology

1 INTRODUCTION

The determination of earthquake source details using seismic waveforms is an integral part of seismological research that has led to advances in our understanding of plate tectonics, earthquake processes and lithospheric stress distributions. Most studies use wavelengths that are large compared to the source dimension in order to apply the point source approximation, which greatly simplifies the process. There are two descriptions of seismic point-sources generally used in source mechanism studies: the classical description of a shear dislocation by a double-couple (DC) with a fault and auxiliary plane (e.g. Dreger & Helmberger 1993) and the more general seismic moment tensor (e.g. Dziewonski *et al.* 1981) which describes body forces in a continuous medium around the point source (e.g. Gilbert 1971; Jost & Herrmann 1989). We use the point source approximation and invert for the seismic moment tensor (MT).

A number of methods have been developed for source-mechanism determination. The simplest use first motion polarity and/or amplitude of body wave signals in observed waveforms (e.g. Hardebeck & Shearer 2003) and usually require a large number of waveforms. While these methods are still used to determine mechanisms in small studies, waveform-matching methods have become more popular for regional or larger scales. A variety of approaches to waveform inversions exist, all relying on the comparison between sections of observed data and synthetically produced waveforms using idealized models of the Earth. MT or DC mechanism inversions can utilize body waves (e.g. Dreger & Helmberger 1993), surface waves (e.g. Romanowicz 1982) and full waveforms (Ekström *et al.* 1998). Both time-domain (e.g. Dziewonski & Woodhouse 1983) and frequency domain inversions (e.g. Romanowicz 1982) have been developed, some of which additionally invert for the centroid or hypocenter location, rupture patterns (finite sources), or the source time function (e.g. Kikuchi & Kanamori 1991; Tocheport *et al.* 2007).

In addition to the development of sophisticated source parameter determination procedures, significant work has been done on using such methods to obtain source details automatically and in real-time or near real-time (Pasyanos *et al.* 1996; Tajima *et al.* 2002; Scognamiglio *et al.* 2009). There are multiple advantages to such systems. First, large numbers of events can be processed and made available for general research purposes with much less effort than previously, even if manual revision or checking is required. Secondly, there is an increasing need to obtain event information soon after the occurrence for emergency response agencies and in some
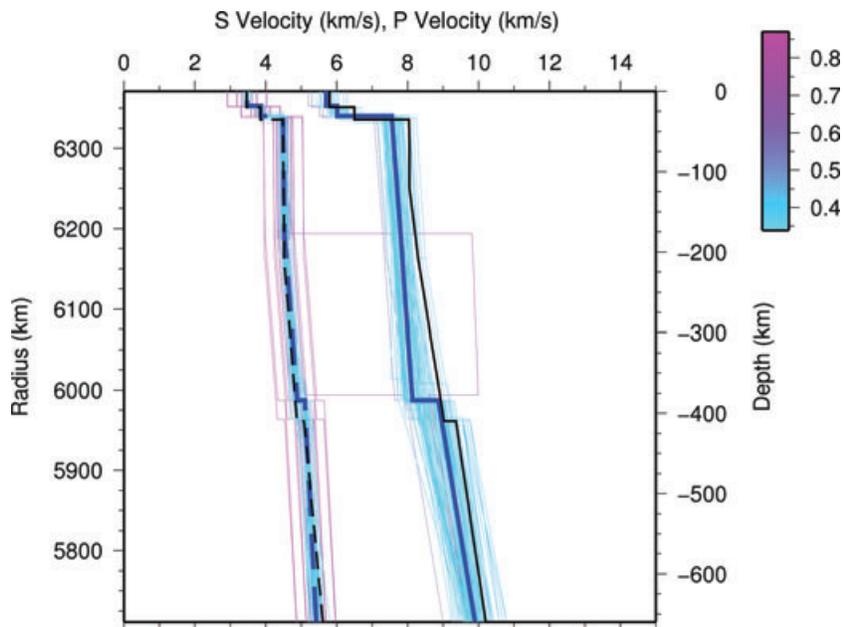
Figure 1. Results of a 20-parameter search by perturbing starting model–ak135 (black lines–*S*-wave velocity on the left, *P*-wave velocity on the right). Coloured lines show models tested and their average misfit (colour scale is shown on right; the lower the misfit the higher the fit). Thick blue lines indicate the best model found, which was only 1 per cent better than starting model.
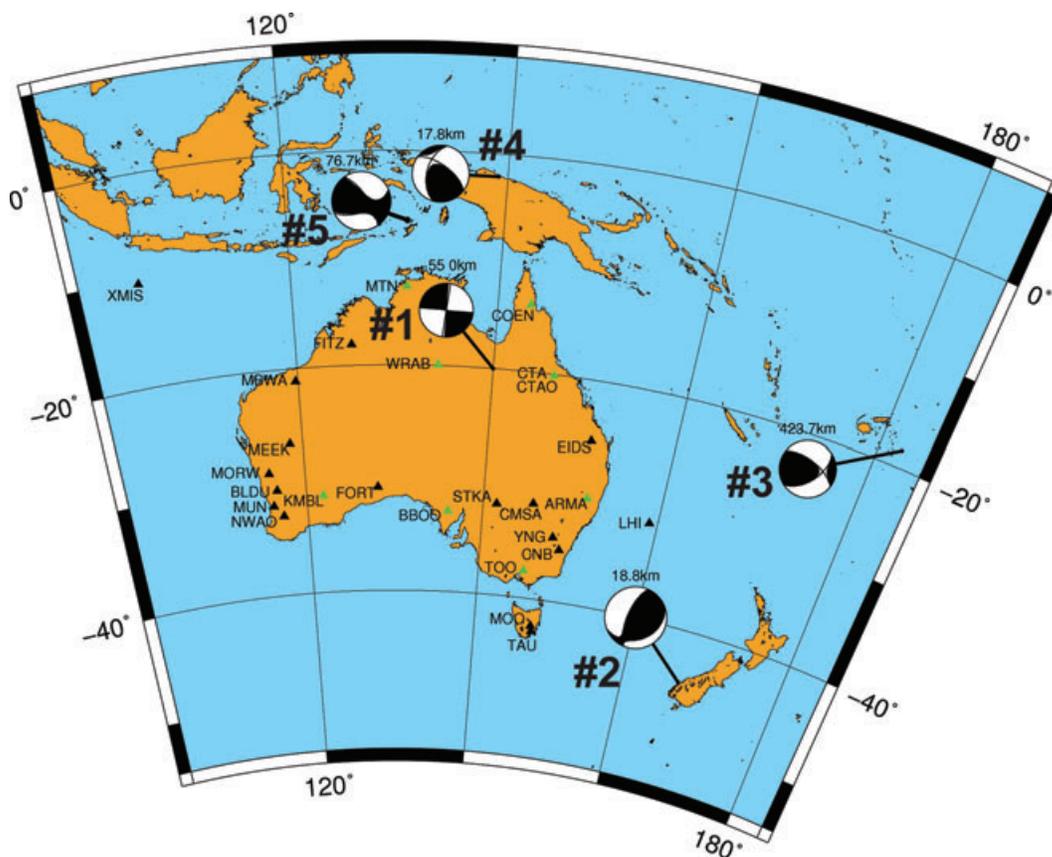

Figure 2. A map of Australasia, showing Australian permanent broadband seismic stations (triangles) and the five sources used in this study (lower-hemisphere projections displayed). Green triangles indicate stations used in the synthetic testing.

areas for tsunami warnings. This is possible over regional distances, utilizing only a few minutes of data, or on slightly larger distances by restricting the inversion to body waves.

In 2005, the Australian Government realized the need for reliable earthquake monitoring to enable an Australian-specific tsunami warning system. Geoscience Australia (GA) operates the Australian National Seismic Network (ANSN), which consists of approximately 50 permanent broadband seismometers across Australia for

the purpose of monitoring seismic activity in the surrounding region. This network combined with over 120 international stations (http://www.bom.gov.au/tsunami/about_jatwc.shtml) allows GA to routinely estimate source parameters in real-time or near real-time (Polet *et al*. 2006). The current tsunami warning system (Australian tsunami warning system) is based only on a determination of earthquake magnitude and location. However, tsunami excitation is strongly dependent on focal mechanism (e.g. Geist
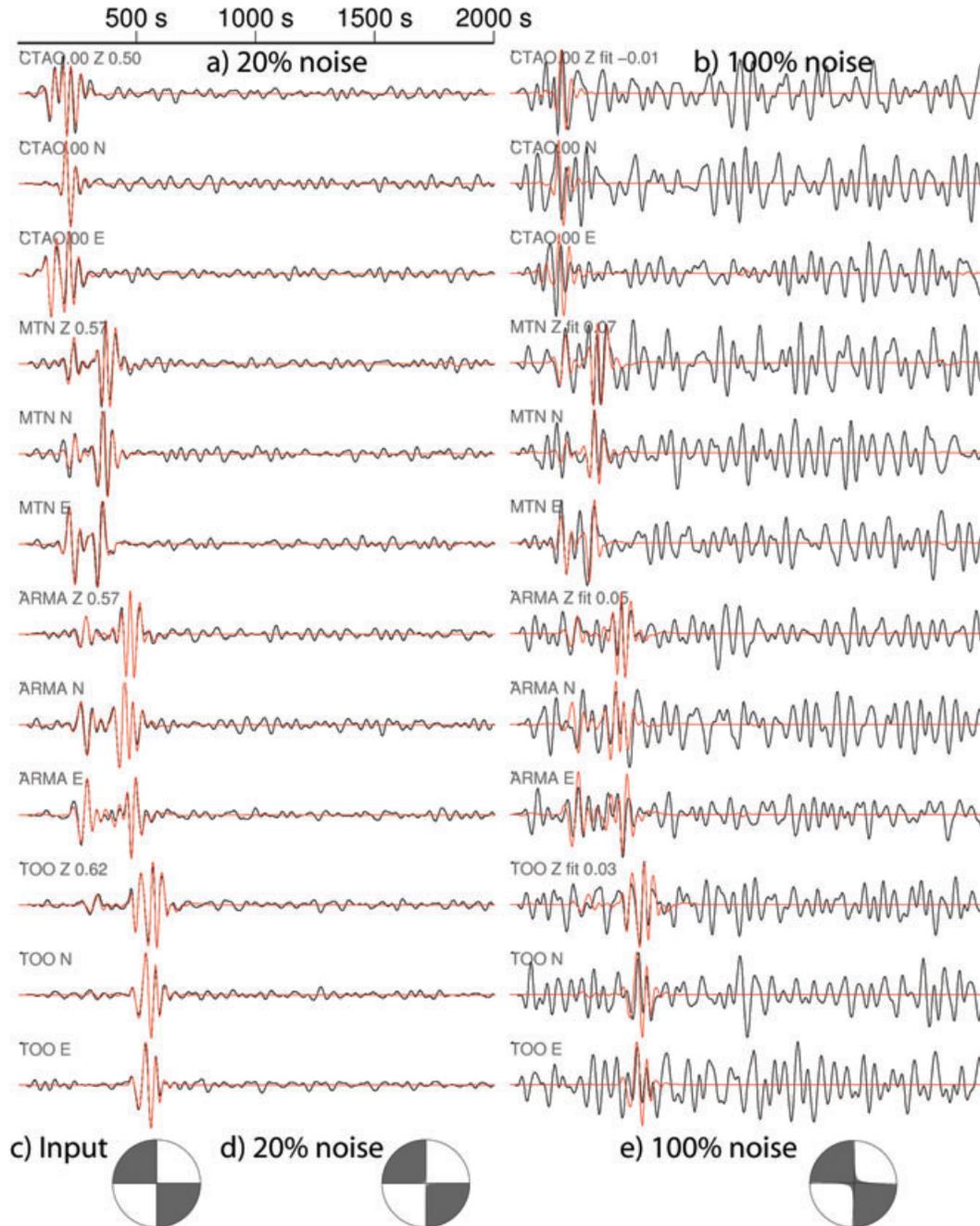

Figure 3. Example results of synthetic test A for event #1 with noise added: moment tensor inversion of synthetic data generated using the 1-D model, with Green's functions generated using the same model. The Green's functions are computed for the exact source location used to produce the synthetic data originally, so there is no error in the location. Waveforms with (a) 20 per cent noise added and (b) 100 per cent noise added for four of the eight stations used (green triangles in Fig. 2), with input data as black traces and output synthetics in red. Station names and components printed and the average goodness of fit for all three components for each station printed with the Z component label; (c) original (input) mechanism used to generate synthetic data (100 per cent double-couple (DC), M5.97); (d) solution mechanism from the inversion with 20 per cent noise (fit 0.53, 99 per cent DC, M5.97); (e) solution mechanism from inversion with 100 per cent noise added (fit 0.04, 93 per cent DC, M5.93).

2005) and it seems certain that next generation tsunami warning systems will make use of more detailed source information such as focal mechanism (e.g. Baba *et al.* 2009). GA established a MT inversion system using real-time data from the ANSN network and international stations. This system (AutoCMT) currently uses a spherically symmetric structural model of the Earth (Kennett *et al.* 1995) without an earth-flattening approximation.

Here we investigate the feasibility of using a 3-D Earth model to perform MT inversion of the events from the Australasian region using GA stations. A 3-D model of the Australasian region has recently been obtained from full waveform tomography (Fichtner *et al.* 2009; Fichtner *et al.* 2010). The model, henceforth referred to as AMSAN.19, includes 3-D crustal structure and radial anisotropy. This eliminates the need of crustal corrections and it allows us to incorporate both Love and Rayleigh wave data in the inversion. A realistic 3-D Q model (Abdulah 2007) is also implemented. The full waveform tomography used a large variety of data, including fundamental- and higher-mode surface waves, long-period body waves and waveforms that could not be identified in terms of classical seismological phases. As a result, AMSAN.19 accurately predicts the complete seismogram and this justifies our full waveform approach to MT inversion.

This is not the first time MT inversion has been performed using a 3-D model. Liu *et al.* (2004) solved for source mechanisms in southern California using spectral-element simulations of regional seismic wave propagation in an integrated 3-D velocity model and Ramos-Martinez & McMechan (2001) found that using a 3-D structural model reduced residual errors by more than 50 per cent (again in California, at regional distances).

2 METHOD

The MT inversion was performed in the time domain using 3-component velocity seismograms for receivers located across Australia (Fig. 3). Multiple vertical (Z), North (N) and East (E) components, bandpass filtered between 40- and 200-s periods and with the instrument response removed, were inverted simultaneously to obtain a seismic MT solution assuming a non-volumetric point source. Recorded seismograms for events around Australia were used to test the inversion program. This data was obtained from IRIS DMC (Incorporated Research Institutions for Seismology Data Management Center; http://www.iris.edu/data) using the BREQ_FAST email request tool and instrument response was removed from the seismograms using the sensor response information provided with the data by IRIS and verified with information available directly from GA. Seismograms were 2000 s long (interpolated to one sample per second), starting at the event origin time, to capture the full waveforms for the farthest stations. Source information that was used for comparison with our solutions was obtained from the GCMT online catalogue. Since 2006, the Centroid-Moment Tensor Project (CMT; Dziewonski *et al.* 1981) has migrated into a new project named 'The Global CMT Project' (GCMT; http://www.globalcmt.org).

2.1 Green's functions using 1-D and 3-D earth models

For each of the Earth models, elastodynamic Green's functions were computed. The Green's functions are defined as theoretical impulse displacement responses of the Earth for a seismic source with orientation given by each corresponding MT element. We can express the displacement for an arbitrary fault mechanism as a linear combination of five MT Green's functions (we constrain the MT to have
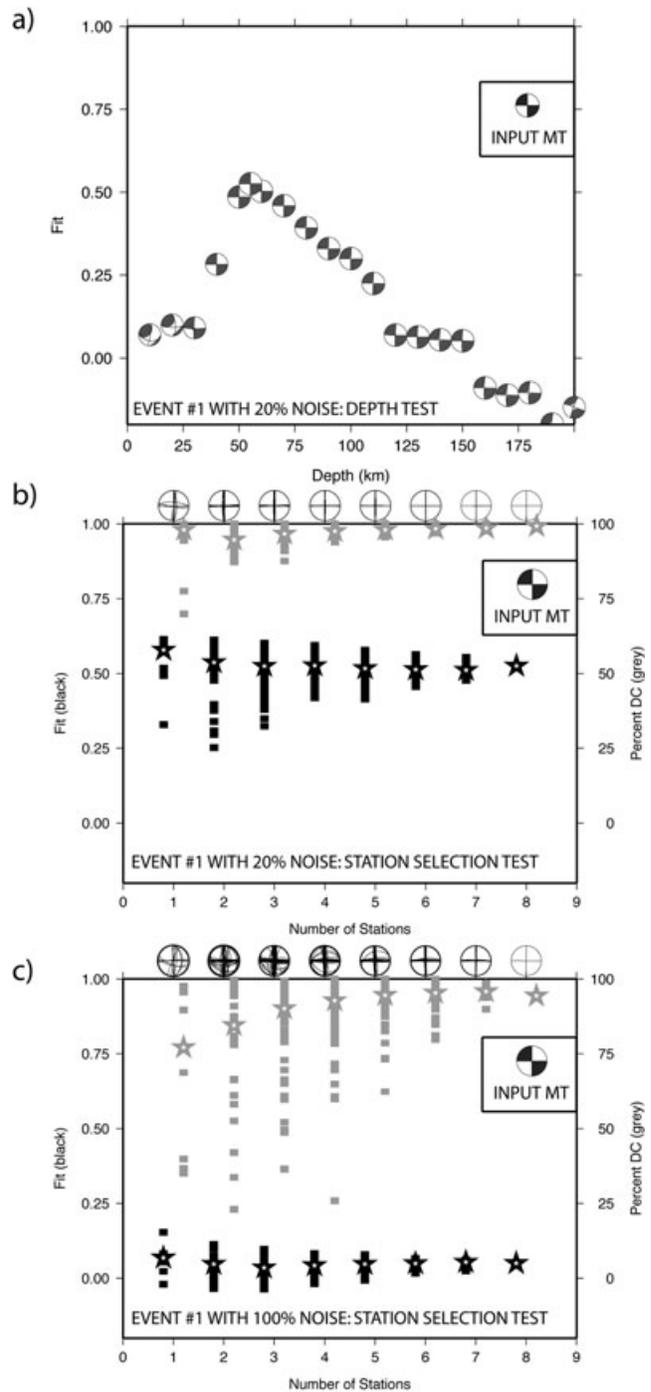

Figure 4. (a) Results of synthetic test B (depth sensitivity test) for event #1 using synthetic data from the 1-D model, with 20 per cent noise added (waveforms shown in Fig. 3). Goodness of fit is plotted against depth assumed in the inversion, while the epicentre is fixed at the correct values. The original source was at 55 km depth; (b) summary of results for synthetic test C (station selection sensitivity test) for event #1, using 1-D synthetic data with 20 per cent noise added. The results are grouped by number of stations used and for each combination the goodness of fit is plotted with a black square and the percentage DC of the solution is plotted with a grey square. At the top of each column, the DC part of each solution (fault planes) are printed overlaid to give an indication of the variability in orientation of the solutions. The median value of fit and percentage DC per cent for each column is indicated with a star; (c) the same as (b) but with 100 per cent noise added to the synthetic data.

zero trace), which is the basis for the MT inversion (e.g. see Jost & Herrmann 1989). The first set of Green's functions were computed by GEMINI (Friederich & Dalkolmo 1995) using the 1-D model PREM (Dziewonski & Anderson 1981), while the second set was computed using the 3-D model AMSAN.19 (Fichtner *et al.* 2010) and the spectral-element code SES3D (Fichtner *et al.* 2009). Green's functions are pre-computed for each source–receiver pair and processed in the same way as the data (interpolation and fil-

tering). We make the assumption that the source time function is a unit impulse; the Green's functions were computed with the source time function included. The computation time to produce a set of Green's functions for a single source location using the 1-D model was around 0.5 to 1 hr on a desktop (using one processor on a Sun Ultra 24, 3.0 GHz Intel Core2 Quad, 4 Gb RAM), while it took 1 to 1.5 hr on the local supercomputer (using 50 nodes, or 200 2.8 GHz processors of TerraWulf II; http://rses.anu.edu.
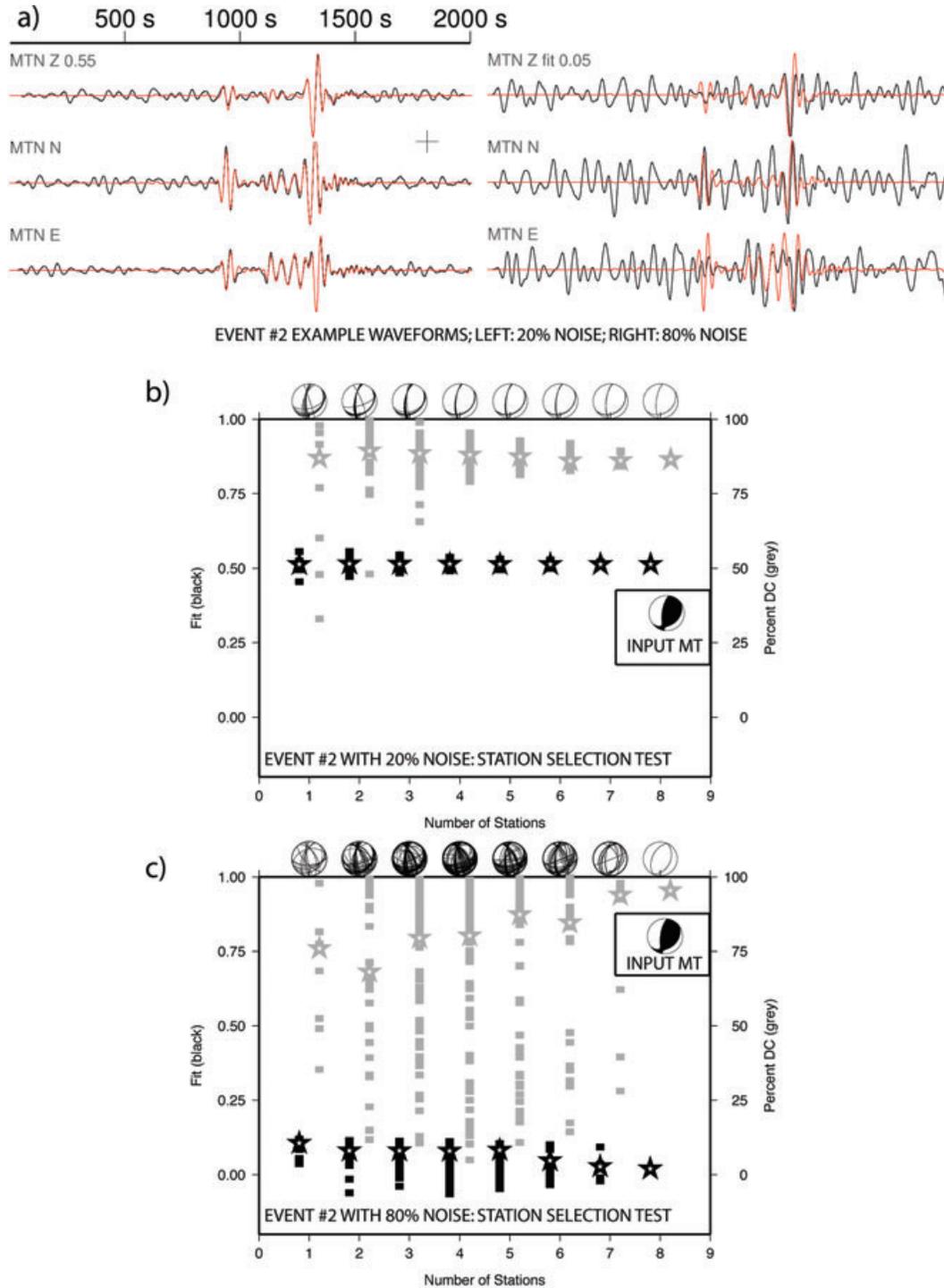

Figure 5. (a) Exemplary waveforms from synthetic test A for event #2 with 20 per cent noise added (left) and 80 per cent noise added (right) to the synthetic data (the same format as in Fig. 3). (b) As Fig. 4(b), showing the results of synthetic test C (station selection sensitivity) for event #2 using synthetic data with 20 per cent noise added. (c) The same as (b) but with 80 per cent noise added to the synthetic data.

au/TerraWulf/) to produce equivalent Green's functions using the 3-D model.

2.2 Synthetic testing method

The method used to compute Green's functions was also employed to generate synthetic data for a number of sources. Uncorrelated, pseudo random noise traces were added to the synthetic data in amounts between 0 and 100 per cent, scaled by maximum amplitude and filtered with the same band-pass filter as the observed data. More specifically, to create noisy waveforms, time-series of 2000 Gaussian random values between –1 and 1 were produced. These were filtered (40–200 s periods) and scaled so that desired ratio was obtained between the maximum amplitudes of the noise and the synthetic data. This roughly imitates signal-to-noise ratios. The use of uncorrelated pseudo random noise leads to an overestimate of the algorithm's performance, whereas since real noise is correlated, it creates constructive interference and forces the inversion to perform less well. Therefore, the use of random noise does not allow us to assess the absolute performance of the algorithm, but it enables us to assess how the 1-D synthetics perform relative to the 3-D synthetics.

2.3. Inversion procedure

The inversion algorithm is based on an already well-established procedure (e.g. Dreger & Helmberger 1993). It was developed keeping in mind an automated application. This was the motivation for using full waveform inversion with a fixed 2000 s window, without phase picking or weighting, or other complications that would require significant manual revision. There were three main stages in the inversion process, which are detailed below.

The first stage is data preparation. Data is loaded for the set of stations to be used and a hypothetical hypocentre is specified. Green's functions corresponding to the source and station locations are loaded from either the 1-D model library or the 3-D model library. This is the only stage in which the method is different when using the 1-D versus 3-D models.

The second stage is determining initial time-shifts. Time-shift for each station is found by cross correlating the appropriate Green's functions and input data. The data was compared with all six corresponding Green's functions (one for each independent element of the MT) and the time-shift was obtained using the one with the best match (the highest cross correlation). The cross correlation formula is given below. Cross correlation C ignores relative size, which removes the need for normalization.

$$C = \left| \frac{\sum_t x(t+\tau)y(t)}{\sqrt{\sum_t x(t)^2 \sum_t y(t)^2}} \right| \tag{1}$$

In the above formula, the first time-series, x, is the data, the second time-series, y, is one of the Green's functions and τ is the time shift.

Applying a time-shift to Green's functions prior to the actual inversion is a procedure that has already been used (see, e.g. Dreger & Helmberger 1993) and is necessary to allow for imperfect travel-times in the model (common when using 1-D), as well as for errors in origin and station times.

The third stage is the actual inversion. The MT is found using linear least square method to solve the equations relating ground movement and Green's functions, that is, the expression of ground movement as a linear combination of Green's functions weighted by the MT (e.g. Jost & Hermann 1989). Goodness of fit is calculated between the input data and synthetic seismograms generated using this MT. This step is repeated and time-shifts varied in a grid-search manner up to 10 s from the values determined in step 2, to maximise the goodness of fit. There is minimal impact on computation cost as the actual inversion is much faster than the first or second stages. The resulting deviatoric MTs were decomposed into DC and
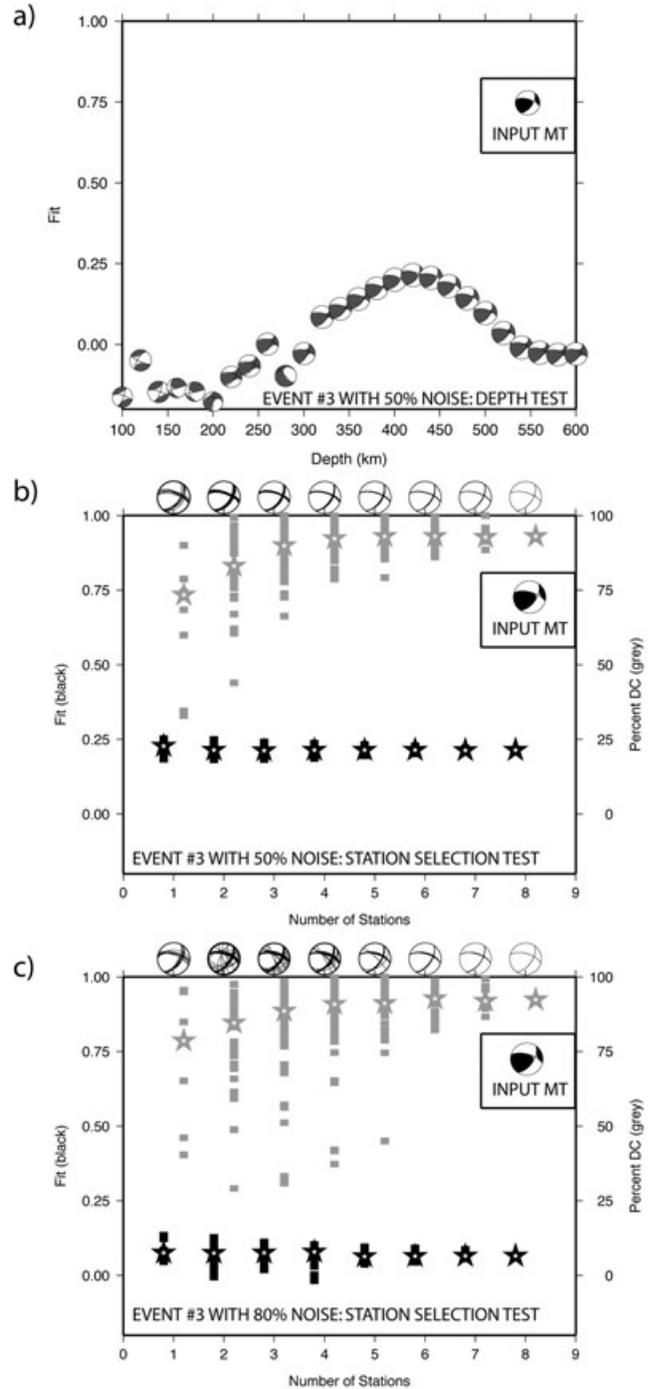

Figure 6. (a) As Fig. 4(a); the results of synthetic test B (depth sensitivity) for event #3 using synthetic data with 50 per cent noise added. (b) As Fig. 4(b); the results of synthetic test C (station selection sensitivity) for event #3 using synthetic data with 50 per cent noise added. (c) The same as (b), but with 80 per cent noise added to the synthetic data.

compensated linear vector dipole (CLVD) components (e.g. Jost & Herrmann 1989).

The goodness of fit F was calculated using the formula below:

$$F = 1 - \sqrt{\frac{\sum\limits_{t}(x(t+\tau)-y(t))^2}{\sum\limits_{t}(x(t))^2}}, \qquad (2)$$

where x is data time-series, y is synthetic time-series, with the time-shift τ and x and y normalized by the maximum amplitude. An empirical 'rule of thumb' determined from studying the inversion results is that goodness of fit above 0.5 is desirable, but fit as low as 0.25–0.30 is still good enough to produce meaningful results. It is important to note that the fit value alone is not a sufficient measure of the quality of the inversion results.

3 THE NEED FOR 3-D EARTH MODELS

An initial study was performed to investigate the possibility of improving existing 1-D models for the Australasian region. It was hoped that tuning global average models using data specific to Australia would result in an improvement in accuracy of synthetics. If sufficient, it would postpone the need to use a 3-D model for accurate MT inversion using the Australian stations. To evaluate the existing Earth reference model, we obtained data from 20 events to the north and east of Australia from the GCMT catalogue that were recorded on permanent broadband stations within Australia. Synthetics were
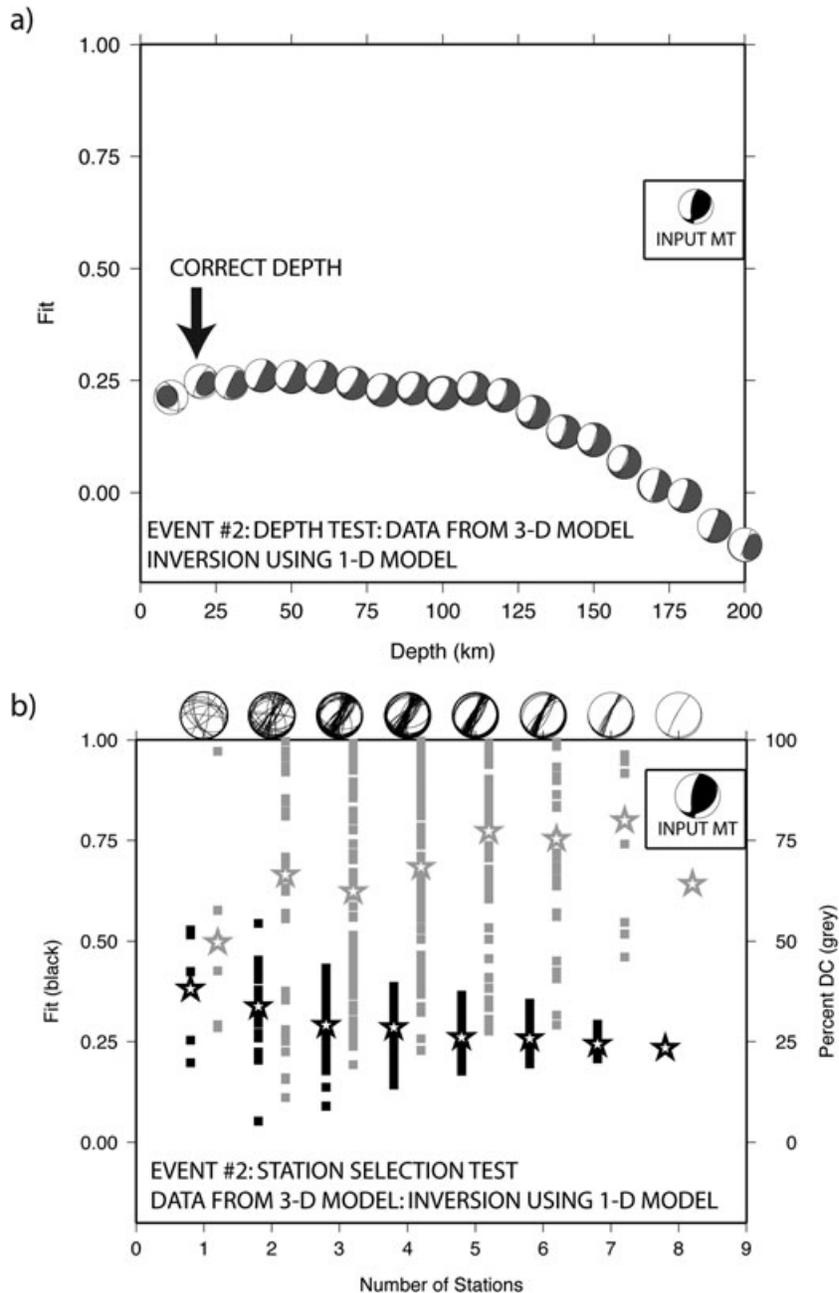

Figure 7. The results of synthetic test of: (a) depth sensitivity; (b) station selection sensitivity, for event #2 using synthetic data (no noise added). Synthetic data are produced using the 3-D model and inverted for the MT solution with synthetics based on 1-D model.

produced using GEMINI (Friederich & Dalkolmo 1995) and the fit between data and synthetics was computed using a formula (2). We started with a simple grid-search over three parameters; crustal velocity, upper mantle velocity and crust–mantle boundary (Moho) depth, with PREM (Dziewonski & Anderson 1981) as the starting model. Velocity in the crust and mantle (to a depth of 660 km) were varied separately by ±10 per cent, and values between 15 km and 40 km were tested for the depth of the crust–mantle boundary (Moho). It was possible to obtain slight improvement over PREM (less than 1 per cent) but this was not considered significant. Similar results were obtained using *ak135* (Kennett *et al.* 1995) as a starting model. The grid-search involved 2000-s long three-component

waveforms, filtered between 40–200 s, but no significant improvement was obtained.

A second study was limited to five events in Indonesia and Papua New Guinea (North of Australia) and the closest 10 Australian recording stations. This dramatically reduced the run time and allowed a much larger number of model parameters to be varied. Two optimisation methods provided by the CADI (Centre for Advanced Data Inference; http://rses.anu.edu.au/CADI/caditk/) were used: a local search, which is essentially a modified grid-search and a recursive hypercubing optimization search. In latter, the parameter space is randomly sampled, as time progresses the size of the parameter space is reduced, focusing on the region with the best fit.
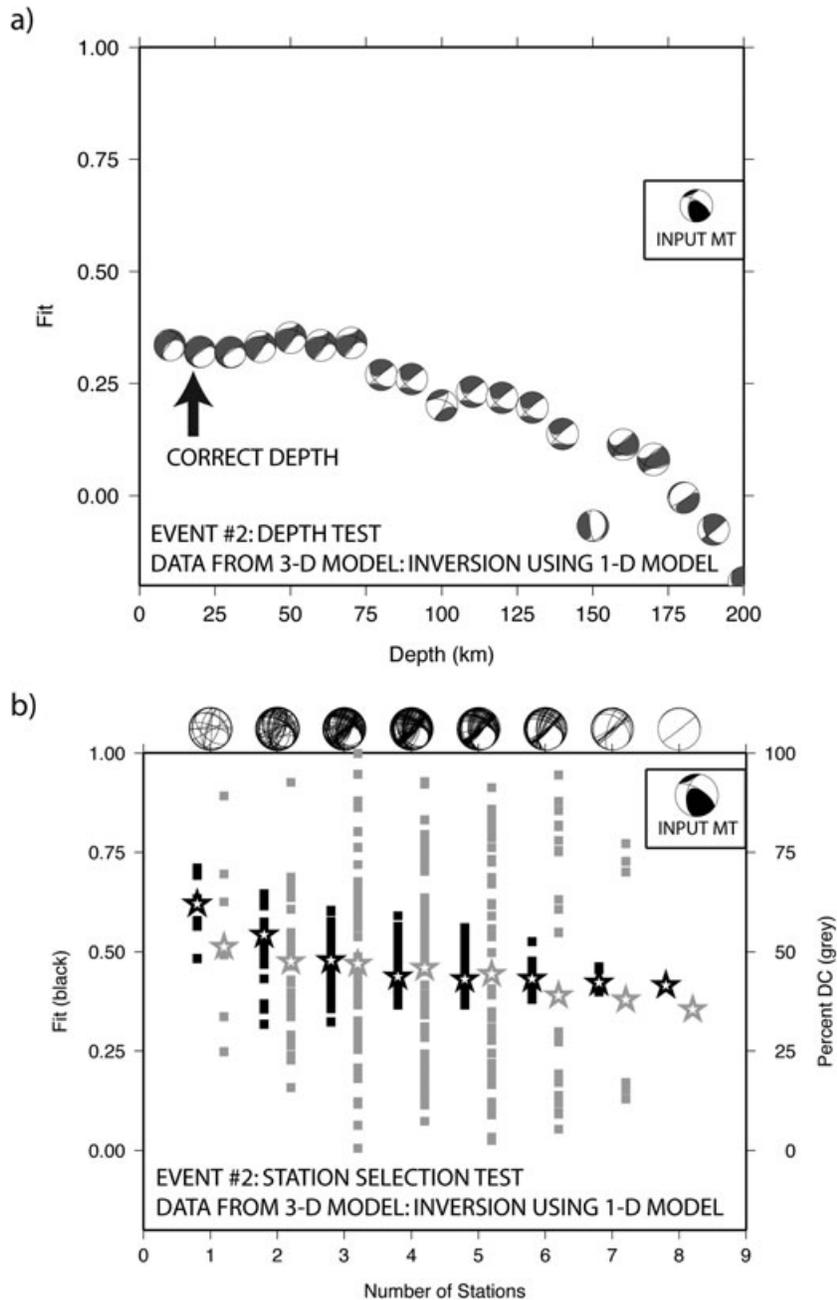

Figure 8. Same as Fig. 7, but for event #4: the results of synthetic test of: (a) depth sensitivity and (b) station selection sensitivity, using synthetic data (no noise added). Synthetic data are produced using the 3-D model and inverted for the MT solution with synthetics based on 1-D model.

A model search was performed for the top 660 km of the Earth, using 20 parameters to define *P*- and *S*-wave velocities and discontinuity depths; four variables are the depths of the layer boundaries, the first two (top) layers have constant *P*-wave velocity, whereas the next three layers have *P*-wave velocity defined by a first degree polynomial, hence eight *P*-wave and eight *S*-wave velocity parameters. Fig. 1 shows the 350 models tested, which again resulted in only a 1 per cent improvement in fit over the reference model.

The above search resulted is unexpectedly small improvement of synthetic waveforms over the reference Earth models. It indicates that Earth structure beneath the Timor and Arafura Seas (between Australia in the south and Indonesia and Papua New Guinea in the north) and the northern part of the Australian continent is well described by the existing reference 1-D Earth models for long wavelengths that were tested. Further improvements in waveform fits are unlikely to be achieved by alternative 1-D structures. To achieve further improvements in waveform fits, a 3-D structural model must be utilized. In addition, the need for a 3-D model in conjunction with MT inversion will be demonstrated in the following section.

4 SYNTHETIC TESTS OF 1-D AND 3-D EARTH MODELS

Tests were performed for a number of synthetic sources (shown in Fig. 2), using subsets of the stations whose waveforms are available (indicated by triangles in Fig. 2). For each synthetic source and amount of noise added, up to three types of MT inversion tests were performed: (A) single inversion using GF's computed for the exact source location used to produce the synthetic data originally, so that there is no error in the location; (B) inversion for a range of depths and exact epicentre (depth sensitivity test); (C) inversion for the exact source location, for every subset of the eight stations (station selection sensitivity test).

4.1 Synthetic sources

Four sources were tested (their mechanisms are shown in Fig. 2) as follows.

(1) Event #1 is chosen as a simple strike-slip source (lat: –20.0; lon: 140.0; H = 55 km; DC = 100 per cent; M = 6.0). This is a purely fictitious event designed to test the basic operation of the program. In this example, the azimuthal coverage is very good, the depth is moderate and the source mechanism is simple.

(2) Event #2 is a realistic source from the GCMT catalogue (lat: –44.71; lon: 167.24; H = 18.8 km, DC = 95 per cent; CLVD = 5 per cent; M = 6.8). This is an event that occurred on the 2007 October 15 near the South Island of New Zealand. The source mechanism and the centroid-location were obtained from the GCMT catalogue, but the data produced was still entirely synthetic.

(3) Event #3 is a source from the GCMT catalogue (lat: –18.46; lon: –177.68; H = 423.7 km; DC = 92 per cent; CLVD = 8 per cent;
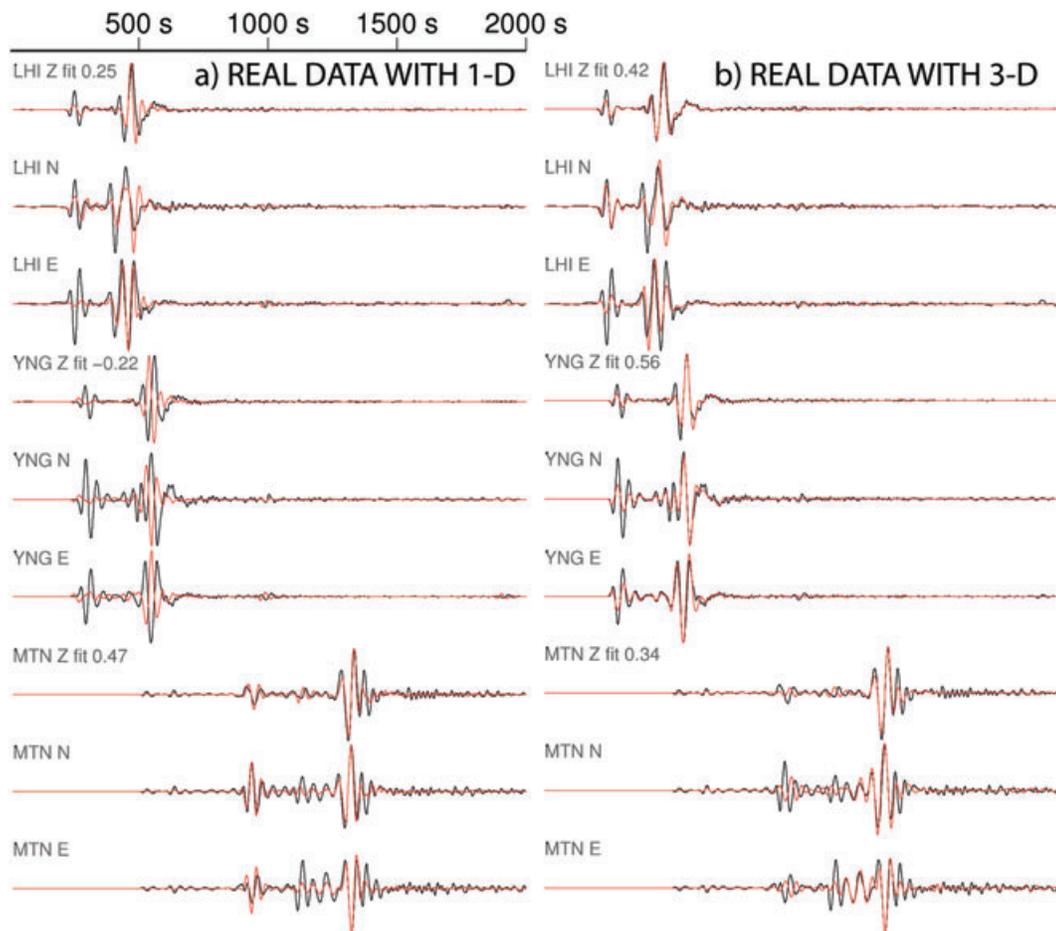

Figure 9. Sample waveforms from the inversion of 'real data' (the observed waveforms) for event #2 using a set of eight stations (three shown), with (a) (left) 1-D synthetics and (b) (right) 3-D synthetics. The format is the same as Fig. 4 (data is shown in black; synthetics are shown in red). Solutions (focal mechanisms, fit level, moment magnitudes and percentage DC) are shown in Fig. 11.

M = 6.3). This is a real event that occurred near Fiji on the 2007 January 8.

(4) Event #4 is also a source from the GCMT catalogue (lat: −2.21; lon: 139.18; H = 17.8 km; DC = 83 per cent; CLVD = 17 per cent, M = 6.2). This is a shallow earthquake that occurred near the north coast of West Papua (Indonesia) on the 2007 December 22.

(5) Event #5 is another source from the GCMT catalogue (lat: −6.59; lon: 131.14; H = 76.7 km; DC = 70 per cent; CLVD = 30 per cent; M = 6.4). This event (2007 December 15 near Tanimbar Islands, Indonesia) is near event #4, but with intermediate depth.

For synthetic sources shallower than 150 km (sources #1, #2, #4 and #5), the depth sensitivity test (test B) was performed for depths from 5 to 200 km; for the deep source (#3), depths between 100 and 600 km were tested. Synthetic tests were per-

formed first with the 1-D model and then comparing the 3-D and 1-D models.

4.2 1-D Synthetic data and 1-D Green's functions

Initial testing of the inversion algorithm was performed using the 1-D model to solve both the forward problem and the inversion. A set of eight stations was used throughout (green triangles in Fig. 2).

The first synthetic source was introduced purely as a way to check the inversion algorithm and the reliability of the sensitivity tests. The results are very good when small amount of noise is added (0 per cent–50 per cent) and the inversion is stable (with an unchanged MT solution and a fully recovered percentage of DC) even with a large amount of noise. A set of example results are provided for synthetic data with 20 per cent and 100 per cent noise
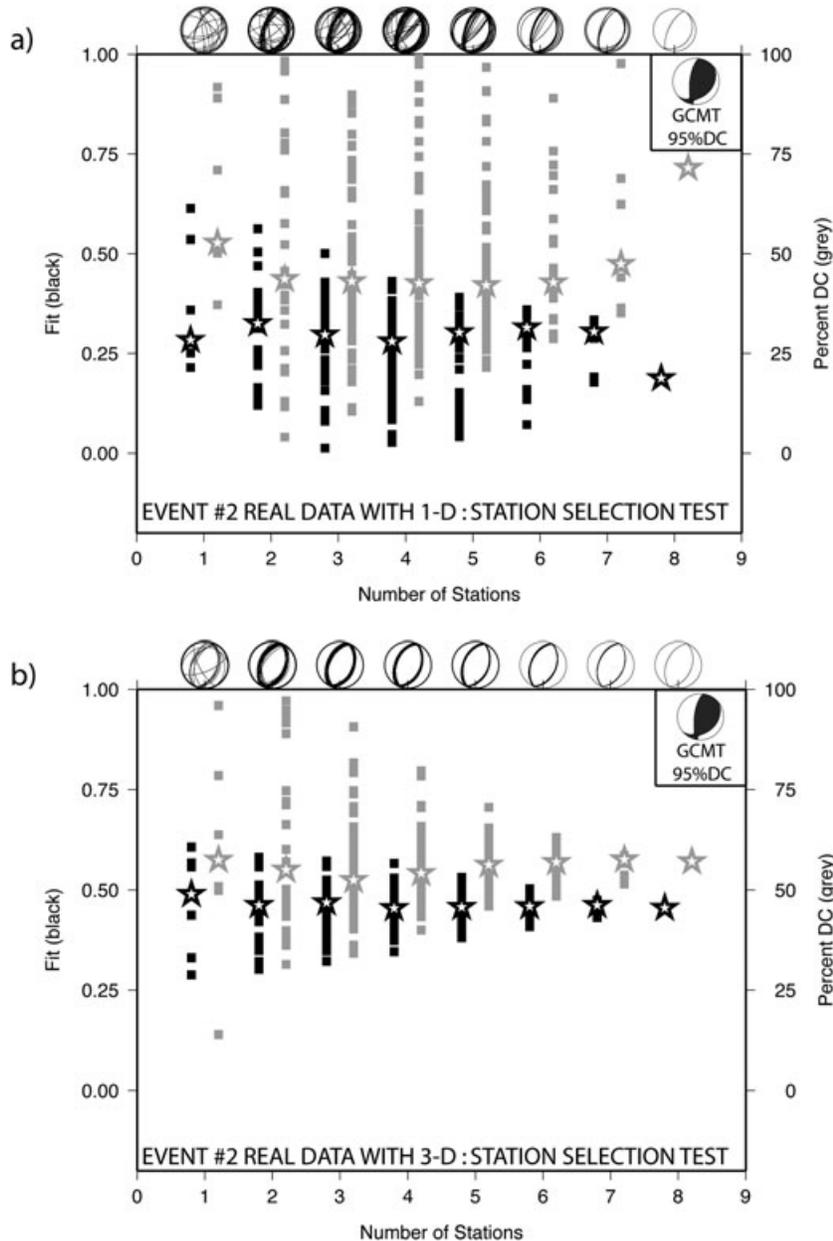

Figure 10. Results of the station selection sensitivity test (synthetic test C; see Fig. 5 for details) using 'real data' (the observed waveforms) for event #2: (a) with 1-D synthetics and (b) with 3-D synthetics. The global CMT solution is included for comparison.

added: waveforms for four of the eight stations used (Figs 3a and b), showing the source mechanism used to generate synthetic data (Fig. 3c) and comparing it to the inversion solutions (Figs 3d and e). The depth sensitivity test with 20 per cent noise has a clear maximum at the correct depth (Fig. 4a) and the station selection sensitivity test shows that even with a single station, the inversion was stable (Fig. 4b). Although the waveform fits were low with 100 per cent noise, the inversion performed well with five or more stations (Fig. 4c) resulting in similar orientation of nodal planes and a fully recovered percentage of DC.

In comparison, the second synthetic source, a shallow event near New Zealand, is much farther from most of the Australian stations and has a much poorer (more realistic) azimuthal coverage. Example waveforms (Fig. 5a) show that it was solved very well with
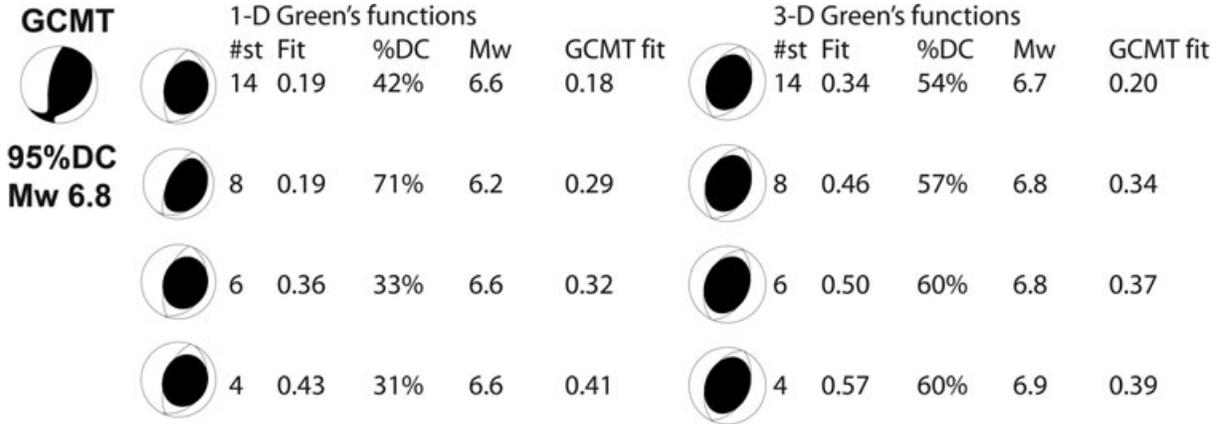

	1-D Green's functions					**3-D Green's functions**				
GCMT	#st	Fit	%DC	Mw	GCMT fit		#st	Fit	%DC	Mw	GCMT fit
	14	0.19	42%	6.6	0.18		14	0.34	54%	6.7	0.20
95%DC	8	0.19	71%	6.2	0.29		8	0.46	57%	6.8	0.34
Mw 6.8											
	6	0.36	33%	6.6	0.32		6	0.50	60%	6.8	0.37
	4	0.43	31%	6.6	0.41		4	0.57	60%	6.9	0.39

Figure 11. The solution mechanisms and details from MT inversion of the observed waveforms for event #2 using 1-D synthetics (left column) and 3-D synthetics (right column) and comparison with the global CMT mechanism (top left). An initial fit is shown in the top row (with 14 stations for both the 1-D and 3-D cases).
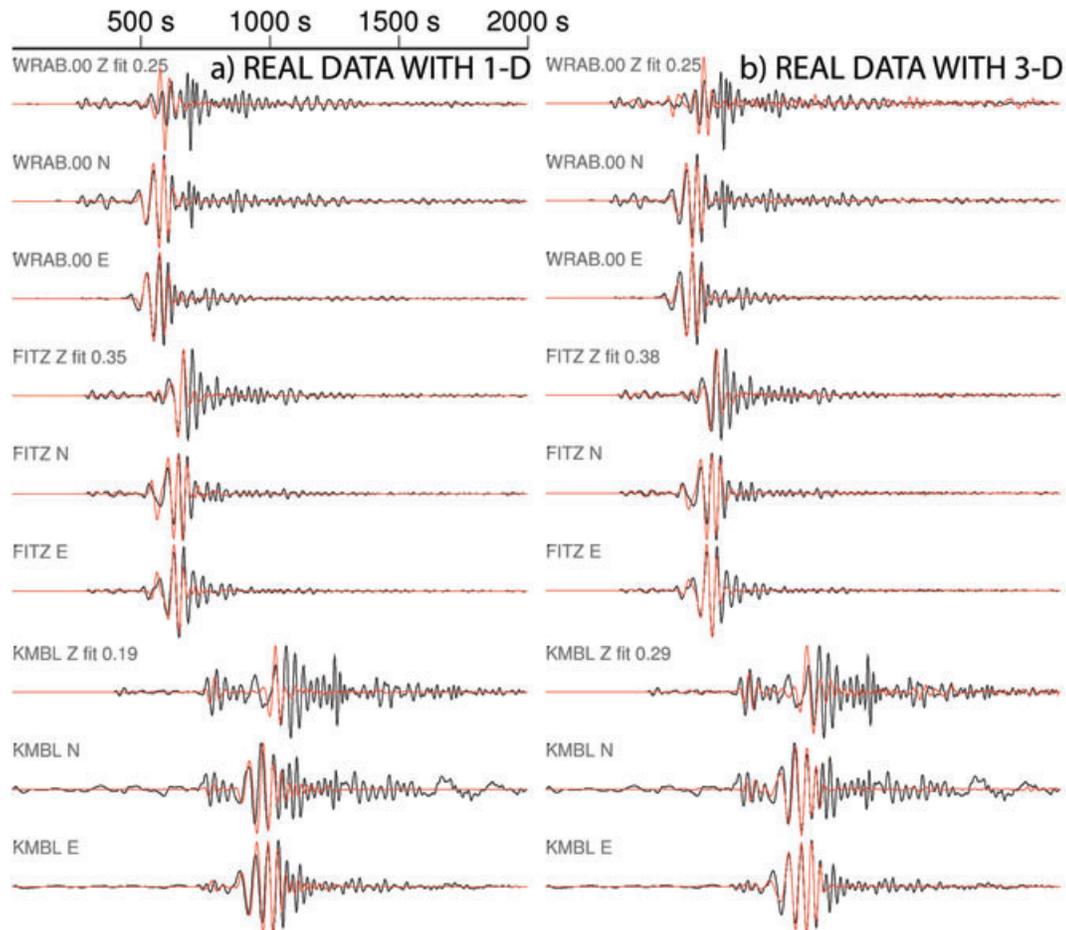

Figure 12. Sample waveforms from the inversion of real data (black lines) for event #4 using a set of eight stations (three shown), with (a) 1-D synthetics (red lines) and (b) 3-D synthetics (red lines). Solutions (focal mechanisms, fit level, moment magnitudes and percentage DC) are shown in Fig. 14.

20 per cent noise (Fig. 5b), but was unstable when 80 per cent noise was added to the synthetic data (Fig. 5c).

The third source mechanism was similar to the second, but deeper (423.7 km). Again, the solutions were almost perfect with 20 per cent noise and still very good at 50 per cent noise (Figs 6a and b). Even at 80 per cent noise, the inversion is stable (Fig. 6c), which is evident in the fact that the orientation of nodal planes does not change significantly with including five or more stations in the inversion. This confirms that the apparent instability for event #2 is due to poor constraint of the source mechanism at shallow depths.

The results of synthetic testing for event #4 were similar to those for event #2, but the fit to the waveforms was worse, perhaps due to the slightly larger CLVD component in the mechanism. Event #5 was not used in synthetic tests.

These synthetic tests show that the inversion is generally robust until the data contains more than 50 per cent noise. Expected fea-

tures of inversion for shallow sources and/or with poor azimuth coverage were observed. In the next section, we investigate how well the 1-D model performs compared to the 3-D model.

4.3 3-D Synthetic data and 1-D Green's functions

One of the key conclusions from our search for the best-fitting 1-D models is that it is difficult to find significantly better 1-D models than the reference Earth models (Dziewonski & Anderson 1981; Kennett *et al*. 1995). Here we want to investigate the uncertainty in MT solutions when such a 1-D model is used to simplify real Earth structure. Therefore we compute synthetic waveforms (synthetic data) using the 3-D model AMSAN.19 (Fichtner *et al.* 2010) and then we deploy 1-D synthetics (1-D Green's functions) computed from the 1-D model to invert for MT. We use the locations of events
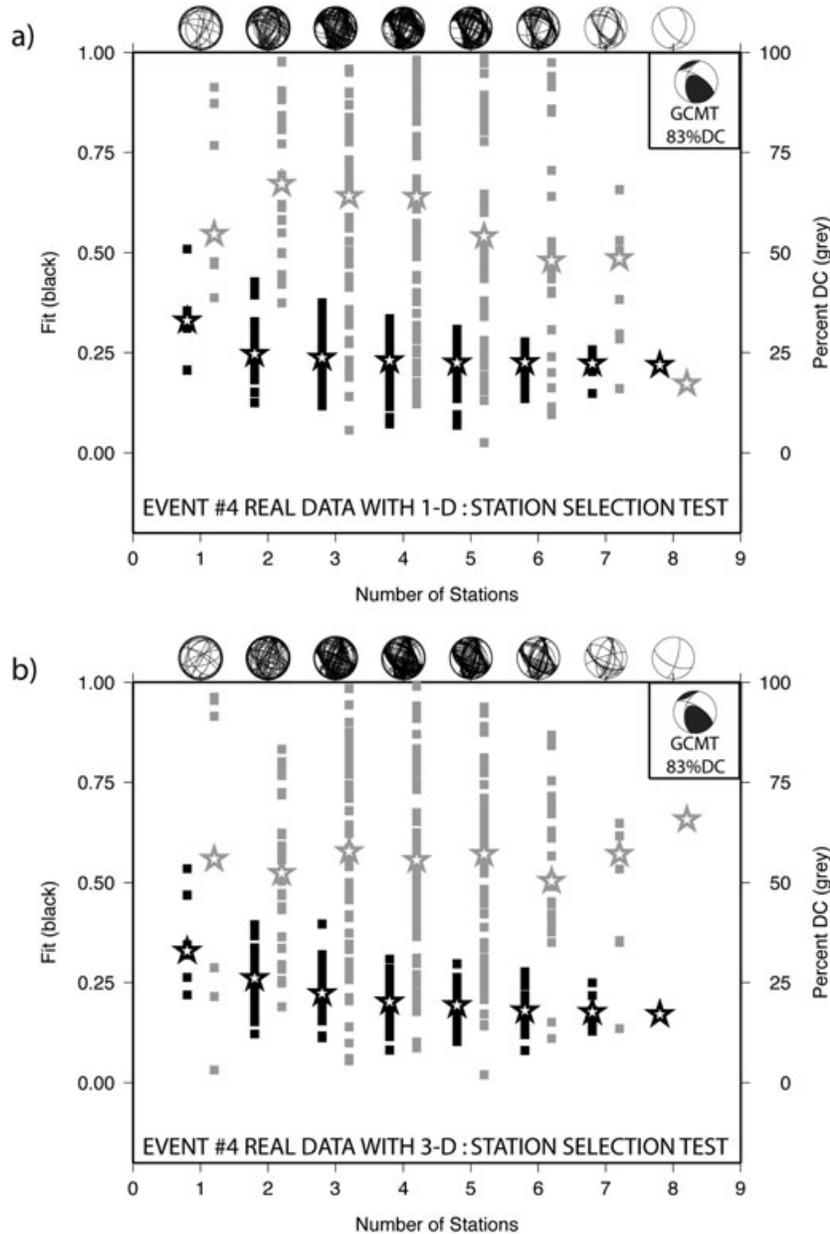

Figure 13. Results of the station selection sensitivity test using real data for event #4: (a) with 1-D synthetics and (b) with 3-D synthetics. The global CMT solution is included for comparison.

and the GCMT source parameters of events #2, #3 and #4 from the previous section to make our synthetic experiment as realistic as possible. No noise was added to the synthetic data, thus the differences in the MT solutions should be solely due to the structural models. Depth and station sensitivity tests (Figs 12 and 13) indicate that the 1-D Green's functions perform very poorly for sources #2 and #4. The fits do not exceed the value of about 0.25 when eight stations are used in the inversion and there is no sensitivity with changing source-depth (Figs 7a and 8a). Station number-sensitivity tests (Figs 7b and 8b) show that at least four to five stations are needed to obtain consistent orientation of principal axes for event #2 and that more than eight stations would be needed for event #4. Also alarming for event #4 is the small percentage of DC, which is an artefact of grossly misrepresented Earth structure.

The above result clearly argues for the need of using 3-D model for the MT inversion wherever possible. 1-D Green's functions are successful for source #3 which may simply be due to the fact that 1-D earth model along ray-paths from Fiji to Australia is representative of the 3-D model, in which case the use of 1-D model is justified.

5 MT INVERSION WITH REAL DATA

Broadband waveforms were obtained for the four events whose source parameters were taken from the GCMT catalogue (events #2, #3, #4 and #5). After processing raw data, the MT inversion was performed using GFs from both the 1-D and the 3-D models. The source locations from the GCMT catalogue were assumed for these inversions (fixed depth and epicentre). Synthetic waveforms were generated using the GCMT mechanism for both the 1-D and 3-D models and compared to the data by calculating the average goodness of fit for the same station combinations as used in the sensitivity tests. The MT solutions were compared with the GCMT mechanisms both visually and numerically.

5.1 Event #2

It was possible to obtain three-component velocity seismograms for the New Zealand event (event #2 in Fig. 2) for 22 of the stations considered. Out of these, eight were discarded in an early stage after a visual inspection due to poor data quality. Considering factors such as goodness of fit, azimuthal coverage and data quality, eight stations were selected for further consideration and an initial MT was obtained using 14 stations.

The best solutions using the 1-D Green's functions and 3-D Green's functions were obtained empirically through a process of station selection. The observed and synthetic waveforms for some of these stations are shown in Fig. 9. All subsets of the eight stations were tested (Fig. 10) and the best solutions for various combinations of stations identified. While the 1-D synthetics perform well during the inversion considering the poor azimuthal coverage and shallow source, the 3-D solutions are always superior. Just as importantly, the station selection sensitivity test (Fig. 10a for 1-D and Fig. 10b for 3-D) clearly illustrates that the inversion using 3-D synthetics is more reliable than the 1-D version.

Fig. 11 shows the focal mechanism solutions (column #1), including the goodness of fit (column #2), the percentage DC (column #3), the moment magnitude (column #4) and the goodness of fit of the GCMT solution (column #5) for the same selected combination of stations. Station selection was performed independently for 1-D and 3-D, generally resulting in slightly different selection of combinations of stations (hence the difference in GCMT fit values in Fig. 11 between 1-D and 3-D). It is worth noting that the resulting synthetic waveforms for the 3-D case have consistently a significantly higher goodness of fit than synthetics from the GCMT solution. The same is not true for the 1-D case (e.g. for eight stations). Furthermore, the moment magnitude obtained using the 3-D model is equivalent to the moment magnitude reported by the GCMT catalogue. The above example illustrates that the earth structure between Australia and New Zealand might not be well represented by the reference 1-D earth model and that a 3-D model should be deployed for the MT inversion.

5.2 Event #3

Event #3 has a small number of usable stations nevertheless the results obtained from the 1-D and 3-D inversions are very similar to those from the GCMT catalogue. In some cases, the 1-D synthetics perform even better than the 3-D synthetics, suggesting that the 1-D model averages Earth structure well east of Australia. Since event #3 is a deep earthquake, it is not surprising that the 1-D model works well, as the lithosphere is not sampled by the body waves on the source side. Furthermore, since surface waves are not present, the goodness of fit is driven by the fit of body waves and in these circumstances it is difficult to make comparisons with event #2.
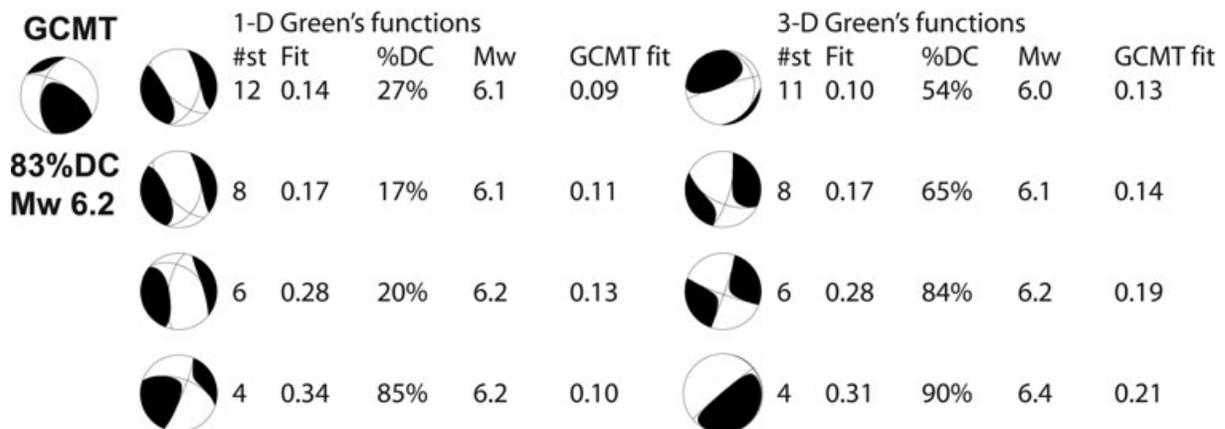

	1-D Green's functions					3-D Green's functions				
GCMT		#st	Fit	%DC	Mw	GCMT fit		#st	Fit	%DC	Mw	GCMT fit

GCMT

83%DC
Mw 6.2

	12	0.14	27%	6.1	0.09		11	0.10	54%	6.0	0.13
	8	0.17	17%	6.1	0.11		8	0.17	65%	6.1	0.14
	6	0.28	20%	6.2	0.13		6	0.28	84%	6.2	0.19
	4	0.34	85%	6.2	0.10		4	0.31	90%	6.4	0.21

Figure 14. The solution mechanisms and details from inversion of real data for event #4 using 1-D synthetics (left column) and 3-D synthetics (right column) and comparison with the global CMT mechanism (top left). An initial fit is shown in the top row (with 12 stations for the 1-D case and 11 stations for the 3-D case).

5.3 Events #4 and #5

We present two more MT inversion analysis for real data, this time for northern events that were recorded well on the Australian stations. The first one was a shallow event in Indonesia, near West Papua (event #4 in Fig. 2). Recorded data was available for 20 stations for this event, of which 15 had data of sufficient quality to use. After the first iteration of station selection, the number of stations was reduced to 12 stations for the 1-D case and 11 for the 3-D case.

Sample waveforms for three of the sets of eight stations are shown in Fig. 12 and the results from the station selection sensitivity tests performed using these stations are displayed in Fig. 13. In general vertical components are fit better with the 3-D model. It is clear that the inversion results are poor in general for both the 1-D and the 3-D cases, however the 3-D case returns a more

realistic DC percentage level. Focal mechanisms for all stations participating in the initial inversion and then for eight, six and four stations (chosen as for event #2) are shown in Fig. 14, along with solution details. It is interesting to note that the focal mechanism solution for the 3-D case looks similar to the GCMT solution with increased numbers of stations, whereas the 1-D case fails to reproduce it. It is assumed that the significant degree of the MT solution variation is at least partially due to a poorer constraint on shallow mechanisms.

The last MT inversion results we present are for event #5, a similar event to #4 but at a greater depth. Here, both the 1-D and 3-D cases are moderately stable (Fig. 15), but the 3-D model clearly performs better. The progression from 14 stations, down to eight, six and finally four (as in the analysis of previous events) confirms the superiority of the 3-D model, though the margin is small (Fig. 16).
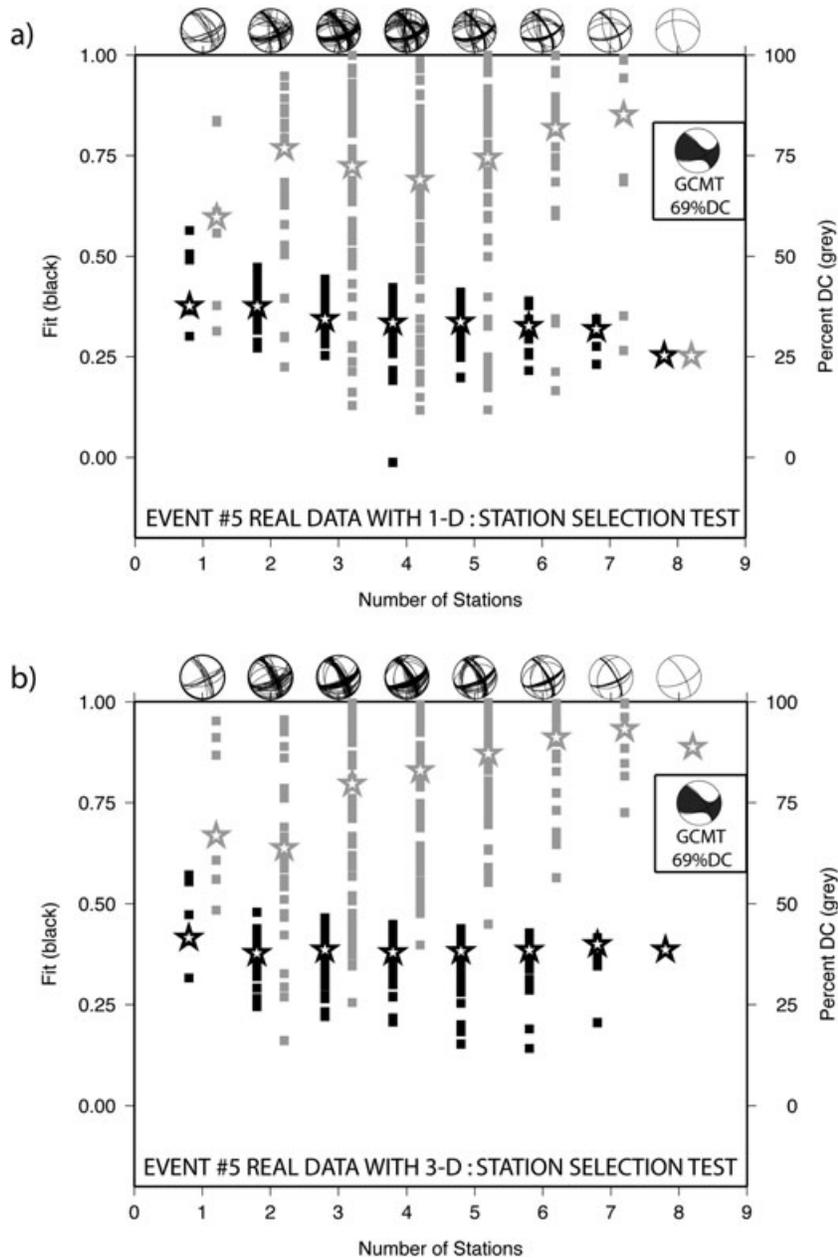

Figure 15. Results of the station selection sensitivity test using real data for event #5: (a) with 1-D synthetics and (b) with 3-D synthetics. The global CMT solution is included for comparison.
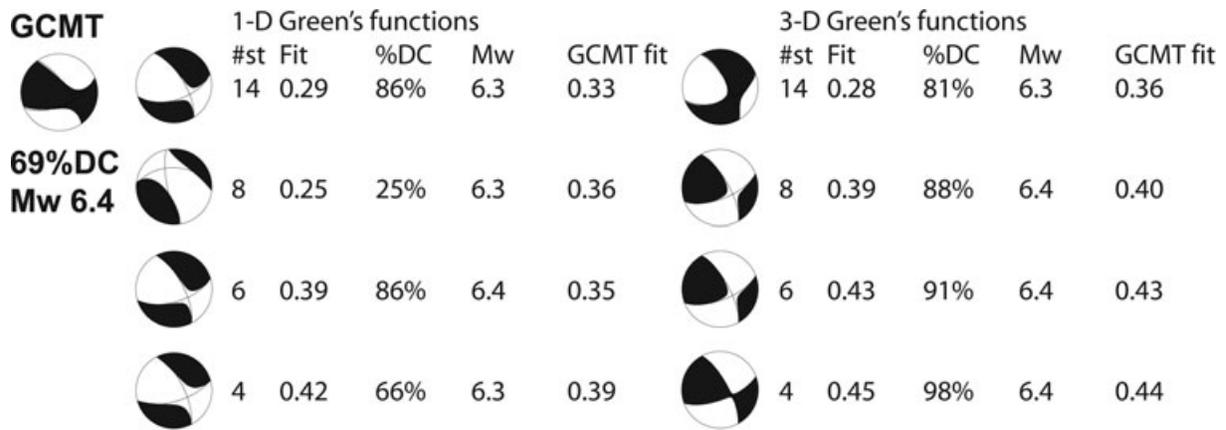
Figure 16. The solution mechanisms and details from inversion of real data for event #5 using 1-D synthetics (left column) and 3-D synthetics (right column) and comparison with the global CMT mechanism (top left). An initial fit is shown in the top row (with 14 stations for both the 1-D and 3-D cases).

6 FUTURE WORK

Depth-sensitivity tests of the sort performed for the synthetic testing with the 1-D model were impractical for the 3-D model due to the much longer run time. Generating 3-D Green's functions for a range of depths and source locations is planned and will take a significant amount of time to complete. These would also be used to test the sensitivity of the inversion to mislocation of the source. Results from such a study are required to determine the appropriate spacing of source locations for coverage of the Australasian area. With a help of a large super-computer, it is hoped that we would be able to roughly cover the seismically active regions near Australia. Constantly increasing computer resources will soon allow us to approach such problems with relative ease.

The current inversion procedure uses full waveforms, however it has been noted that this is dominated by surface waves. It would be interesting to investigate the advantages of a surface-wave only inversion, which is predicted to improve accuracy and slightly reduce computation time.

7 CONCLUSIONS

We have designed a MT inversion scheme using 3-component seismic waveforms to efficiently study earthquakes in the Australasian region. Initial synthetic tests with the 1-D model (PREM) only, indicate the method performs well for fixed depths even with large amounts of additive random noise. We investigated the need for using a 3-D structural model of the region, compared to standard approaches relying on 1-D models. Inversions using 1-D Green's functions did not recover the correct source parameters from synthetic data generated by the more realistic 3-D model and were only successful for the synthetic event near Fiji. This indicates that, in some areas, the 1-D model may approximate well the real Earth structure. However, the key result of the study is that 3-D waveform modelling and MT inversion should be facilitated whenever possible to retrieve realistic source parameters. Furthermore, we tested our method using real data from earthquakes in the region around Australia and compared results with the GCMT solutions. It is apparent that MT inversion is improved by the use of 3-D Green's functions in some cases, but further work needs to address and improve the reliability for other locations.

Future improvements are aimed at increasing the general efficiency of the method. It may be that this method will be used as a compliment to other methods such as W-phase inversion. This was a first but important step towards a fully automated MT inversion procedure to utilize national and stations surrounding Australian region.

REFERENCES

Abdulah, A., 2007. Seismic body wave attenuation tomography beneath the Australasian region, *PhD thesis*, The Australian National University.

Baba, T., Cummins, P.R., Thio, H.K. & Tshushima, H., 2009. Validation and joint inversion of seismic waveforms for earthquake source modelling using deep ocean bottom pressure records: a case study of the 2006 Kuril megathrust earthquake, *Pure Appl. Geophys.,* **166**(1), 55–76.

Dreger, D. & Helmberger, D., 1993. Determination of source parameters at regional distances with three-component sparse network data, *J. geophys. Res.,* **98**, 8107–8125.

Dziewonski, A.M. & Anderson, D.L., 1981. Preliminary reference Earth model, *Phys. Earth planet. Int.,* **25**, 297–356.

Dziewonski, A.M. & Woodhouse, J.H., 1983. An experiment in systematic study of global seismicity: centroid-moment tensor solutions for 201 moderate and large earthquakes of 1981, *J. geophys. Res.,* **88**, 3247–3271.

Dziewonski, A.M., Chou, T.-A. & Woodhouse, J.H., 1981. Determination of earthquake source parameters from waveform data for studies of global and regional seismicity, *J. geophys. Res.,* **86**, 2825–2852.

Ekström, G., Morelli, A., Boschi, E. & Dziewonski, A.M., 1998. Moment tensor analysis of the central Italy earthquake sequence of September-October 1997, *Geophys. Res. Lett.,* **25**(11), 1971–1974.

Fichtner, A., Kennett, B.L.N., Igel, H. & Bunge, H.-P., 2009. Full seismic waveform tomography for upper-mantle structure in the Australasian region using adjoint methods, *Geophys. J. Int.,* **179**, 1703–1725.

Fichtner, A., Kennett, B.L.N., Igel, H. & Bunge, H.-P., 2010. Full waveform tomography for radially anisotropic structure: new insight into present and past states of the Australasian upper mantle, *Earth planet. Sci. Lett.,* **290**, 270–280.

Friederich, W. & Dalkolmo, J., 1995. Complete synthetic seismograms for a spherically symmetric Earth by a numerical computation of the Green's functions in the frequency domain, *Geophys. J. Int.,* **122**(2), 537–550.

Geist, E.L., 2005. Rapid tsunami models and earthquake source parameters: far-field and local applications, *ISET J. Earthq. Technol., 42,* 127–136.

Gilbert, F., 1971. Excitation of the normal modes of the Earth by earthquake sources, *Geophys J. R. astr. Soc., 22,* 223–226.

Hardebeck, J.L. & Shearer, P.M., 2003. Using S/P amplitude ratios to constrain the focal mechanisms of small earthquakes, *Bull. seism. Soc. Am.,* **93**(6), 2434–2444.

Jost, M.L. & Herrmann, R.B., 1989. A student's guide to and review of moment tensors, *Seismol. Res. Lett.,* **60**(2), 37–57.

Kennett, B.L.N., Engdahl, E. & Buland, R., 1995. Constrains on the velocity structure in the Earth from travel times, *Geophys. J. Int.,* **122,** 108–124.

Kikuchi, M. & Kanamori, H., 1991. Inversion of complex body waves – III, *Bull. seism. Soc. Am.,* **81,** 2335–2350.

Liu, Q., Polet, J., Komatitsch, D. & Tromp, J., 2004. Spectral-element moment-tensor inversions for earthquakes in southern California, *Bull. seism. Soc. Am.,* **94,** 1748–1761.

Pasyanos, M.E., Dreger, D.S. & Romanowitcz, B., 1996. Toward realtime estimation of regional moment tensors, *Bull. seism. Soc. Am.,* **86**(5), 1255–1269.

Polet, J., Thio, H.K., Earle, P., Cummins, P.R. & Bathgate, J., 2006. Near real-time determination of earthquake source properties and tsunami potential using long period surface waves, *EOS, Trans. Am. geophys. Un.,* **87**(52), Fall Meet. Suppl., Abstract S13B–0222.

Romanowicz, B., 1982. Moment tensor inversion of long period Rayleigh waves: a new approach, *J. geophys. Res.,* **87,** 5395–5407.

Ramos-Martinez, J. & McMehan, G.A., 2001. Source-parameter estimation by full waveform inversion in 3-D heterogeneous, viscoelastic, anisotropic media, *Bull. seism. Soc. Am.,* **91**(2), 276–291.

Scognamiglio, L., Tinti, E. & Michelini, A., 2009. Real-Time Determination of Seismic Moment Tensor for the Italian Region, *Bull. seism. Soc. Am.,* **99,** 2223–2242.

Tajima, F., Megnin, C., Dreger, D.S. & Romanowicz, B., 2002. Feasibility of real-time broadband waveform inversion for simultaneous moment tensor and centroid location determination, *Bull. seism. Soc. Am.,* **92,** 739–750.

Tocheport, A., Rivera, L. & Chevrot, S., 2007. A systematic study of source time functions and moment tensors of intermediate and deep earthquakes, *J. geophys. Res.,* **112,** B07311, doi:10.1029/2006JB004534.